






Article

Improvements on the Carrier-Based Control Method for a Three-Level T-Type, Quasi-Impedance-Source Inverter

Fermín Barrero-González ¹, Carlos Roncero-Clemente ^{1,*}, María Isabel Milanés-Montero ¹,
Eva González-Romera ¹, Enrique Romero-Cadaval ¹, Oleksandr Husev ² and V. Fernão Pires ³

¹ Department of Electrical, Electronic and Control Engineering, School of Industrial Engineering, University of Extremadura, 06006 Badajoz, Spain; fbarrero@unex.es (F.B.-G.); milanes@unex.es (M.I.M.-M.); evagzlez@unex.es (E.G.-R.); eromero@unex.es (E.R.-C.)

² Department of Electrical Engineering, School of Engineering, Tallinn University of Technology, Ehitajate tee 5, 19086 Tallinn, Estonia; oleksandr.husev@ieee.org

³ D INESC-ID and Setúbal School of Technology, Polytechnic Institute of Setúbal, Setúbal, Portugal; vitor.pires@estsetubal.ips.pt

* Correspondence: croncero@peandes.net; Tel.: +34-924289600

Received: 10 May 2019; Accepted: 13 June 2019; Published: 14 June 2019



Abstract: The boost feature that characterizes Z-source and quasi-Z-source converters is usually achieved by means of a proper insertion of short-circuit states in the full DC-link. In this work, a novel pulse width modulation carrier-based strategy for a three-phase, three-level T-type, quasi-Z-source inverter is introduced, based on the addition of alternate short-circuits in the two halves of the DC-link bus. This technique achieves better performance, less electromagnetic interference, and lower harmonic distortion of the output line-to-line voltage compared to the traditional methods based on the full DC-link shoot-through. At the same time, generating the switching states is to easy implement. The proposed strategy permits the use of electronic devices with lower blocking voltage capability, thus improving converter reliability, size, and cost. The new method may be implemented in another multilevel inverter with an impedance-source network as well. A comprehensive simulation study is performed in order to validate the adopted method, with different inverter input voltages, which is taken as representative of a photovoltaic array. Comparisons are conducted with conventional strategy insertions using the same topology in order to show the improvements achieved.

Keywords: impedance-source converters; multilevel; pulse width modulation (PWM); T-type inverter; three-level T-type, quasi-impedance-source inverter (3L-T-type qZS inverter)

1. Introduction

The two-level, three-phase voltage source inverter (VSI) is probably one of the most widely used power electronic converters. Its area of application includes photovoltaic (PV) systems or drives for AC electric machines. Three-level VSIs have also been studied and used as an alternative to the standard two-level inverter because they offer a lower electromagnetic interference level, better waveform quality, lower semiconductor stress, and increased efficiency at higher switching frequencies [1–3]. Among the three-level VSI topologies, two main groups can be distinguished: the three-level, neutral-point clamped (3L-NPC) topology and the three-level T-type (3L-T-type) topology. The T-type inverter only uses one bidirectional power switch for clamping the middle node to the positive or negative DC-link, and it requires two diodes less per bridge leg [4]. As the external semiconductors of the T-type inverter must block the total DC-link voltage, the NPC variant seems a more suitable choice at higher switching frequencies, when switching losses become more significant [1]. However, both groups of inverters

have voltage buck features, i.e., they are unable to provide an output AC voltage higher than the DC bus voltage. In practical applications such as PV systems, a DC/DC boost converter is required in front of the inverter. However, this solution is more complex and difficult to control.

Unlike two-stage topology, a single-stage inverter is an attractive, compact, and reliable choice. With the aim of overcoming traditional VSI handicaps, impedance source (Z-source) inverters emerge as a different family characterized by the inclusion of boosting capability within the inversion operation. An impedance source network, made up of two capacitors and two inductors connected to both DC bus terminals in Z-shape, provides a coupling between the inverter and the DC input source. This arrangement permits the use of the so-called shoot-through (ST) state, which the input voltage boost to be achieved and, consequently, broadens application fields. This type of inverters increases input voltage limits [5], which is a typical condition in a PV system. Furthermore, the possibility of including short circuit states in the inverter-bridge branches as well as the removal of dead times contributes to improving system reliability and the quality of output waveforms. A wide research contribution has been reported in the literature since the first proposal by Peng [6]. A complete overview of the different Z-source topologies, their improvements, and different arrangements is presented in [7]. Compensation methods for three-level Z-source inverters under semiconductor failure conditions are proposed in [8]. As an evolution of the Z-source inverter, a new topology called quasi-impedance-source (quasi-Z-source) inverter was proposed in [9]. A study of the various impedance network topologies can be found in [10]. A combination of two symmetrical quasi-Z-source networks with a 3L-NPC inverter was studied in [5,11]. A comprehensive analytical comparison of the Z-source- and quasi-Z-source-based two- and multilevel inverters was presented in [12] in terms of passive component sizing and semiconductor stress. With the main aim of improving the performance obtained with the previous impedance-based 3L-NPC topology, the combination of two quasi-Z-source networks with the active 3L-NPC inverter was presented in [13]. This paper proved that a higher efficiency and a better distribution of switching losses among the switches was achievable. Reference [14] presented the association of two symmetrical quasi-Z-source networks with a T-type inverter that could operate both under regular and semiconductor fault situations. A comparison of three-phase, three-level VSIs with intermediate DC/DC boost converters and three-level quasi-Z-source inverters was reported in [15]. A slightly different topology that included two additional switches in the quasi-Z-source network was studied in [16].

Two-level, three-phase Z-source inverter modulation techniques were reviewed and compared in [17,18]. A space vector modulation (SVM) method of a 3L-NPC Z-source inverter was developed in [19]. In [20], the switching sequence was modified to balance neutral-point potential. A new SVM applied to a single-phase, 3L-NPC Z-source inverter with a reduced number of conversions, higher performance, and equally distributed switch losses among transistors was recently proposed in [21]. Reference [22] proposed an SVM scheme for a 3L-T-type quasi-Z-source inverter with the aim of reducing the value and slew rate of common-mode voltage. A more advanced version of the previous SVM scheme was found in [23]. Besides common-mode voltage reduction, the neutral-point voltage balance is assured by a proper voltage vector selection strategy. Authors in [24] introduced a carrier-based modulation proposal for a 3L-T-type quasi-Z-source inverter with the ability of generating fixed-width ST states along the whole fundamental period and, in addition, balancing the neutral-point voltage. A modulation technique that combined high- and low-frequency carrier signals in a single-phase, quasi-Z-source, two-level inverter was used in [25]. References [26,27] deal with a two-level, quasi-Z-source inverter; the former applies a modulation technique to control the common-mode voltage, and the latter studies the design aspects to achieve a wide range of operation. Finally, a new trend in the switching strategies based on a finite set of modulation index values and model-predictive control approaches is being studied [28]. This technique is intended mainly for grid-connected applications of the 3L-NPC Z-source inverter.

As previously stated, the Z-source and quasi-Z-source key idea is the insertion of the so-called ST states, which correspond to DC-link short circuits. This is the only possible ST in a two-level inverter.

But, in a three-level inverter, a half DC-link short circuit is also possible. Therefore, besides the full shoot-through (FST) state previously mentioned, two new switching states emerge for three-level inverters: upper shoot-through (UST) and lower shoot-through (LST). These states were defined in [29]; the idea was applied to a 3L-NPC Z-source inverter [19], to a 3L-NPC-quasi-Z-source inverter [30], and to a 3L-T-type Z-source inverter [20]. Moreover, literature pieces dealing with the concept of UST/LST states have all used the modulation-based SVM technique. However, the association of a double quasi-Z-source network with a T-type inverter using a carrier-based modulation technique with UST/LST states has not been considered so far. In this work, a novel, pulse width modulation carrier-based technique for a three-phase, three-level T-type, quasi-Z-source inverter (3L-T-type qZS inverter) is introduced. It consists of the addition of the so-called UST and LST states, which achieves better performance, less electromagnetic interference (EMI), and lower harmonic content of the output voltage signal compared to modulation that uses only the FST state. It also permits the use of electronic devices with less blocking voltage capability, thus improving converter reliability and cost. The control method can be readily adapted to single-phase, multilevel-based, or other impedance source inverters.

The main contributions of this paper are:

- Proposal of a carrier-based pulse width modulation able to generate alternating UST and LST states for a multilevel Z-source, which provides several benefits (aforementioned) compared to the conventional FST state strategies presented in [5,11,24].
- Development of the strategy as a carrier-based pulse width instead of SVM-based, as others reported in the literature [22,23,30], allowing easier implementation.
- Application of the proposed strategy in a three-phase, 3L-T-type qZS inverter. This topology is considered quite promising for renewable energy applications [23,24], and it is validated by simulation.

The rest of this paper is organized as follows. The new modulation technique is developed in detail in Section 2. The theoretical ideas are tested by simulation in Section 3. Section 4 concludes this paper.

2. Theoretical Analysis

The power circuit is shown in Figure 1. Two identical quasi-Z-source networks are connected to a common node between capacitors C_2 and C_3 . These networks are linked to a T-type three-level VSI.

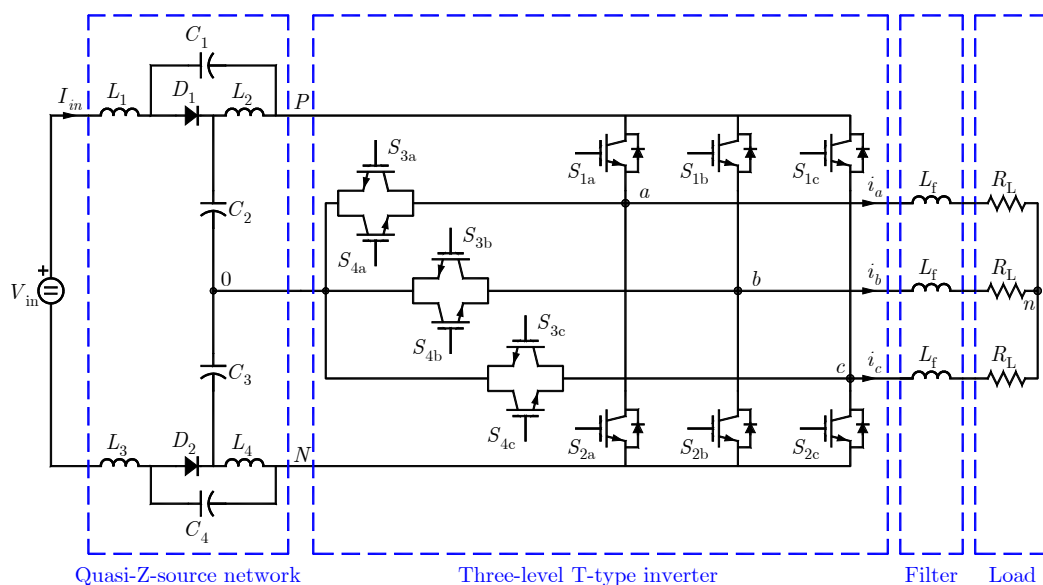


Figure 1. Schematic of the three level (3L) T-type, quasi-Z-source inverter.

2.1. Operation Principle with Upper and Lower Shoot-Through States

By means of diverse switching combinations, a voltage waveform with three possible voltage levels, $-V_{PN}/2$, 0 , and $V_{PN}/2$, was obtained at each converter leg. In the switching scheme used in a traditional three-level VSI, the output of each phase (a, b, c) can be in either P-, 0-, or N-state (i.e., connected to the positive (P), the neutral (0), or the negative (N) terminal, respectively). Three phases and three states were combined to form 27 valid switching states, depicted in Figure 2, in the well-known space vector representation for a three-level converter.

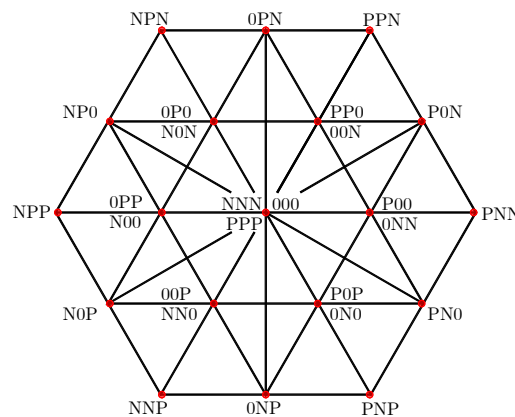


Figure 2. Space vector model of switching states for a three-level inverter.

There was one extra zero state when the load terminals were shorted through the on state of both the upper and lower switches (S_1 and S_2) of any phase leg, combinations of any two phase legs, or all three phase legs. This ST zero state was not allowed in the traditional VSI because it caused a short circuit of the capacitors on the DC side. However, thanks to the quasi-Z-source network, ST states were allowed. Energy was stored in the inductors during ST states. Then, during the non-shoot-through (NST) states (comprising the 27 states of the conventional three-level VSI inverter), it was transferred to the capacitors and the load. By means of adjusting the ST duty cycle, the peak DC-link voltage was controlled, and, therefore, the inverter was provided with the desired buck-boost feature.

The ST state described was the so-called full shoot-through (FST) mode, in which short-circuits in the full DC-link, connecting terminals P with N, were produced. Besides the FST state used in the majority of the previous works, two new switching states named UST and LST states emerged in [29]. The UST state corresponds to the simultaneous activation of switches S_1 and S_3 in a phase leg. It produces a short circuit in the upper half DC-link, connecting terminals P and 0. On the other hand, the LST state takes place when switches S_4 and S_2 in a phase branch are simultaneously turned on. This produces a short circuit in the lower half DC-link, connecting the terminals 0 and N. Application of these new states reduces the harmonic distortion of the output line-to-line voltage compared to the FST. Table 1 describes the mentioned states for the phase- a case. Figure 3 includes the three equivalent circuits in NST, UST, and LST states, respectively.

Table 1. Switches turned on and phase-leg voltage.

| State | ON Switches (Phase a) | V_{a0} |
|---------------------------|----------------------------------|-------------|
| P | S_{1a}, S_{4a} | $V_{PN}/2$ |
| 0 | S_{3a}, S_{4a} | 0 |
| N | S_{2a}, S_{3a} | $-V_{PN}/2$ |
| Full shoot-through (FST) | $S_{1a}, S_{2a}, S_{3a}, S_{4a}$ | 0 |
| Upper shoot-through (UST) | S_{1a}, S_{3a} | 0 |
| Lower shoot-through (LST) | S_{2a}, S_{4a} | 0 |

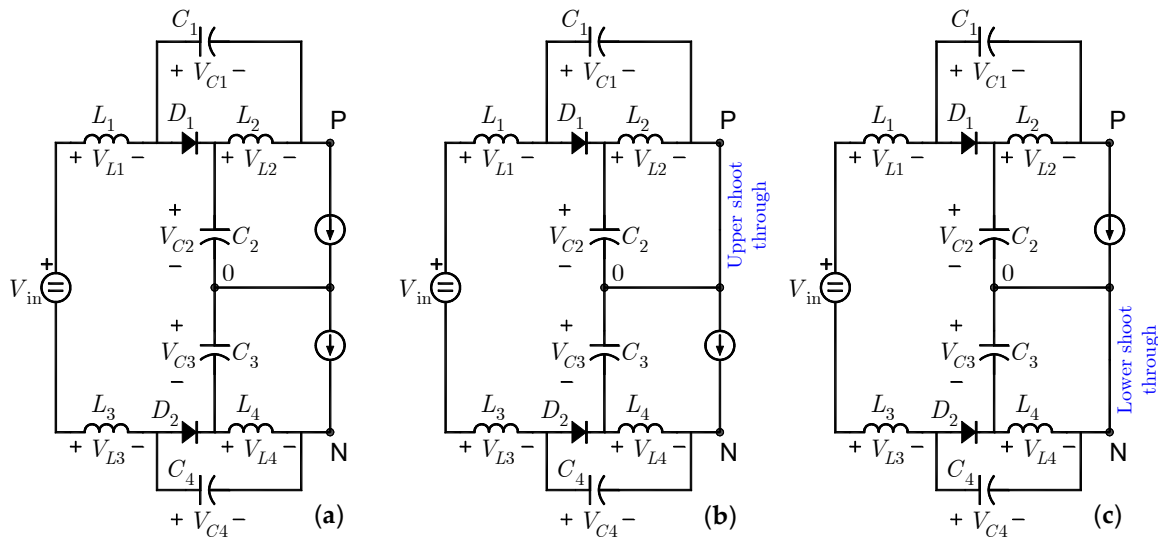


Figure 3. Equivalent circuits for (a) non-shoot-through (NST) state, (b) upper shoot-through (UST) state, and (c) lower shoot-through (LST) state.

T_N , T_U , and T_L define NST, UST, and LST state durations, respectively. The corresponding duty ratios are $D_N = T_N/T$, $D_U = T_U/T$, and $D_L = T_L/T$, where T is the switching period $T = T_N + T_U + T_L$. With the aim of ensuring symmetric operation, D_U and D_L are set to be equal $D_U = D_L = D_0$. If the quasi-Z-source network is assumed to be symmetric (i.e., $L_1 = L_3$, $L_2 = L_4$, $C_1 = C_4$, and $C_2 = C_3$), the voltages across the inductors and capacitors are $V_{L1} = V_{L3}$, $V_{L2} = V_{L4}$, $V_{C1} = V_{C4}$, and $V_{C2} = V_{C3}$. Continuous conduction mode was assumed for the converter operation as well. Then, as the average voltage across inductors during one switching period should be zero in steady state, the boost factor (defined as $B = \hat{V}_{PN}/V_{in}$, where \hat{V}_{PN} is the peak DC-link voltage, present during NST states) can be calculated by the following Equation, [30]:

$$B = \frac{\hat{V}_{PN}}{V_{in}} = \frac{1}{1 - 2D_0}. \tag{1}$$

Therefore, the amplitude of the fundamental output phase-to-neutral voltage is given by

$$\hat{V}_{an,1} = m \frac{\hat{V}_{PN}}{2} = m \frac{1}{1 - 2D_0} \frac{V_{in}}{2}, \tag{2}$$

where m is the modulation index.

2.2. New Carrier-Based Modulation Method

A carrier-based level-shifted PWM (LS-PWM) with a modified constant boost control (MCBC) was proposed. Details of this novel modulation technique application are discussed below.

The reference and carrier signals are displayed in Figure 4 for the case of $m = 0.7$ and $D_0 = 0.1$. A switching frequency value of 500 Hz (i.e., a frequency modulation index $m_f = 10$) was used for better visualization. Three modulating signals v_a^* , v_b^* , and v_c^* were used as in the traditional PWM scheme. These signals were obtained by using the well-known technique based on the addition of a common offset voltage, V_{off} , to the three phase references [17,31]:

$$V_{off} = -\frac{\max(v_a, v_b, v_c) + \min(v_a, v_b, v_c)}{2}. \tag{3}$$

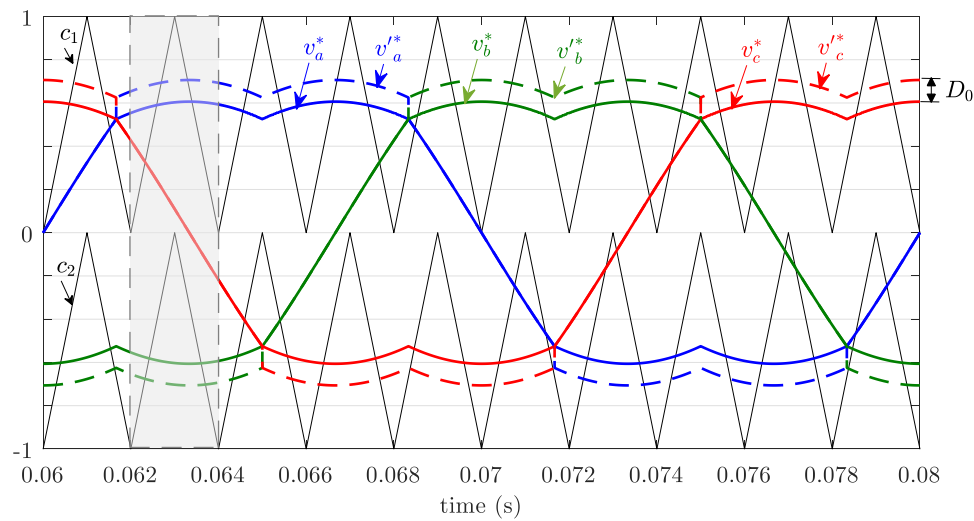


Figure 4. Modulating and carrier signals for one fundamental cycle, where $m = 0.7$, $D_0 = 0.1$, and $m_f = 10$.

This approach permitted the modulation index m to be increased, avoiding the problems associated with overmodulation. In addition, it improved the waveform quality and reduced the switching losses significantly [32].

Another three modulating signals, v_a^* , v_b^* , and v_c^* , were generated by shifting up and down the envelope of v_a^* , v_b^* , and v_c^* by the ST duty cycle (D_0). Then, the switching signals (including the ST states) were obtained by comparing the two sets of modulation signals with the two vertically disposed in-phase carrier signals, c_1 and c_2 , generating the upper and lower ST states (just one phase-leg; a , b , or c was shot-through).

Gate signal generation for switches S_{1x} to S_{4x} ($x = a, b$, and c) is demonstrated in Figure 5 for the switching cycle highlighted in Figure 4 (0.0620 s to 0.0621 s). S_{3x} and S_{2x} would have complementary states to S_{1x} and S_{4x} , respectively, if there were no ST states. The existence of those states (UST and LST) can be observed on the overlapping of the corresponding on-states, pointed out in Figure 5.

By using these six reference signals, the converter was modulated as follows: for a phase-leg x , S_{1x} was turned on when v_x^* was greater than c_1 , and S_{3x} was turned on when v_x^* was smaller than c_1 . On the other hand, S_{2x} was turned on when v_x^* was smaller than c_2 , and S_{4x} was turned on when v_x^* was greater than c_2 .

It is interesting to note that to maintain the volt-second average per switching cycle, UST states should be added into the inverter states with the P terminal unconnected. These states are called N-type small vectors in [20], and they are the states P00, PP0, 0P0, 0PP, 00P, and POP in Figure 2. Similarly, LST states should be added into the inverter states with the N terminal unconnected (i.e., into the so-called P-type small vectors: 0NN, 00N, N0N, N00, NN0, 0N0). One can notice that when the N- and P-type small vectors contain two 0-states, UST and LST states can be achieved in two different ways, depending on the leg used to implement the ST condition. All the UST and LST states are collected in Table 2, where the letters L and U have been introduced in order to distinguish the NST states, and they must be interpreted as the connection of the corresponding phase-leg to the N or P terminal, respectively. This can be verified in Figure 5, where the states are POP, P00, PN0, 0N0, PN0, P00, and POP. UST insertion was performed in the state 0N0, while LST insertion was carried out in states POP and P00.

Table 2. Upper shoot-through (UST) and lower shoot-through (LST) states.

| UST | UNN | U0N | 0UN | NUN | NU0 | N0U | NNU | 0NU | UN0 |
|-----|-----|-----|-----|-----|-----|-----|-----|-----|-----|
| LST | PL0 | PPL | 0PL | LPP | L0P | PLP | 0LP | P0L | LP0 |

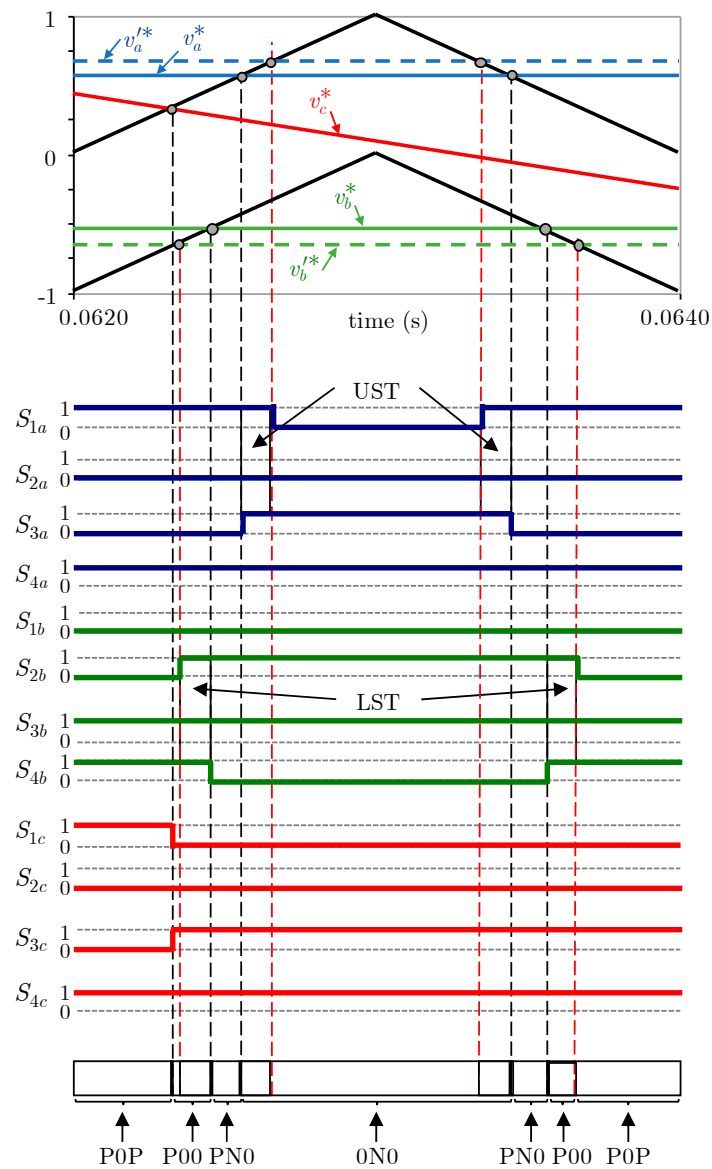


Figure 5. Reference, carrier, and gate signals of the proposed modulation scheme for the switching cycle T (0.0620 s to 0.0621 s) highlighted in Figure 4.

3. Simulation Results

The proposed approach was tested through a simulation study using the PSCAD (version X4 (4.5), Manitoba HVDC Research Centre, Winnipeg, Canada, 2014) simulation tool. The parameters of the chosen quasi-Z-source network (Figure 1) were $C_1 = C_2 = C_3 = C_4 = 470 \mu\text{F}$ and $L_1 = L_2 = L_3 = L_4 = 0.5 \text{ mH}$, and the switching frequency was set at 10 kHz. A DC power supply of 500–800 V was used as inverter input, emulating the operation of a PV array. The converter supplied a balanced, three-phase, wye-connected resistive load, $R_L = 40 \Omega$, at 230/400 V and 50 Hz. A simple inductive filter was used with inductance $L_f = 7.5 \text{ mH}$.

Simulation results of input voltage and current (V_{in} , I_{in}), DC-link voltage (V_{PN}), line-to-line voltages before filtering (v_{ab} , v_{bc} , and v_{ca}), and output currents (i_a , i_b , and i_c) are shown in Figure 6 for the nonboosting case and in Figure 7 using the novel application of UST/LST pulse with modulation approach. In order to show the improvements achieved, the traditional FST strategy was tested by simulation, and the main waveforms were shown in Figure 8. These cases are discussed in the following paragraphs.

First, it was assumed that the output voltage of the PV array was at its maximum value of 800 V. In this case, to synthesize the required output grid voltage (in the range 380–420 V line-to-line RMS), the modulation index and UST/LST duty cycle were fixed to $m = 0.8$ and $D_0 = 0$. Boost operation was not needed, so the inverter operated in the VSI mode. Figure 6 shows the simulated waveform for this case. The current drawn from the PV array (I_{in}) was almost ripple-free since no shoot-through states were activated. The DC-link voltage (V_{PN}) was not boosted ($B = 1$), and it was maintained at almost 800 V. The output line-to-line voltages ($v_{a,b,c}$) were composed of the levels 0, $\pm 800/2$ V, and ± 800 V. The RMS value of the fundamental component was 390.9 V, which was within the desired range. The corresponding phase-to-neutral peak voltage of 319.16 V matched the expected value, according to Equation (2).

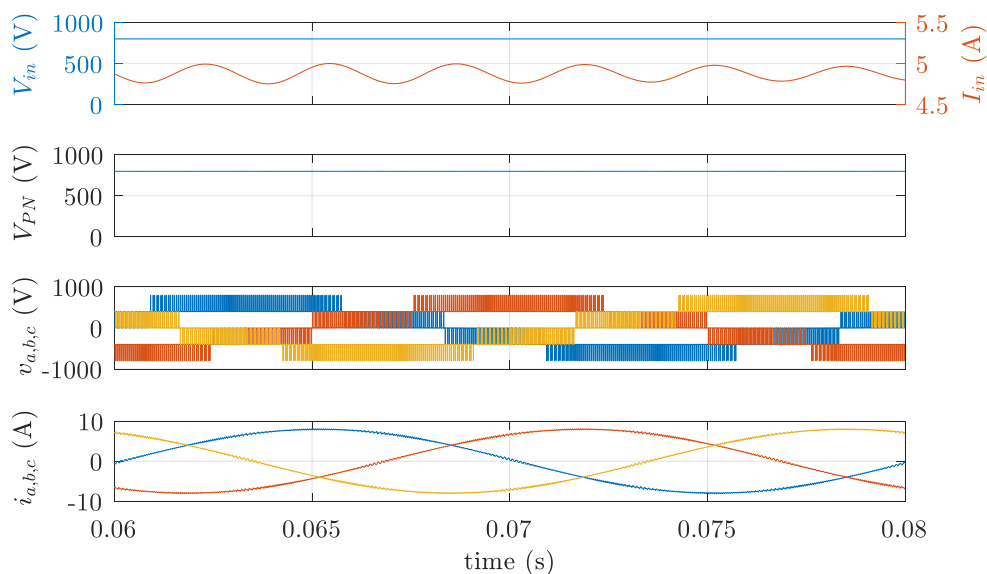


Figure 6. Simulation results for the UST/LST strategy, switching frequency 10 kHz, $m = 0.8$, and $D_0 = 0$. Top to bottom: input voltage (V_{in}) and input current (I_{in}); DC-link voltage (V_{PN}); and line-to-line voltages before filtering (v_{ab} , v_{bc} , and v_{ca}) and output currents (i_a , i_b , and i_c).

Next, to illustrate the boost performance operation, the PV panels output was at its minimum value of 500 V (due to bad weather, for example). Now, to synthesize the required output voltage to the grid, a boost operation was needed. This was achieved by maintaining the modulation index at 0.8 and changing the ratio D_0 to 0.2. The results are shown in Figure 7. Now, the current from the PV array was in continuous conduction mode, with ripples resulting from the shoot-through states. The DC-link voltage was boosted, assuming two levels: BV_{in} and $BV_{in}/2$, where $B = 1/(1 - 2D_0)$ was the boost factor (i.e., almost 827 V and 827/2 V). This was a unique feature of the UST/LST strategy, while for the FST strategy the levels were BV_{in} and 0. The output line-to-line voltages were composed of the levels 0, $\pm BV_{in}/2$, and $\pm BV_{in}$ (i.e., 0, $\pm 827/2$, and ± 827 V). The RMS value of the fundamental component was in this case 404.9 V, which was within the desired range. According to Equation (2), the corresponding phase-to-neutral peak voltage of 330.6 V was in good agreement with the expected value. In both cases, high-quality sinusoidal line currents were also obtained.

It is interesting to note that there were slight errors between the expected and simulated values, since the voltage dropped across the diodes and the inductors L_1 and L_2 were not considered when deriving the equations.

To show the waveform differences and the improved harmonic performance of the proposed UST/LST strategy, compared to the FST strategy, a simulation test using the FST strategy was also carried out. In this case, an FST duty cycle $D_s = 0.2$ was applied. The results are shown in Figure 8.

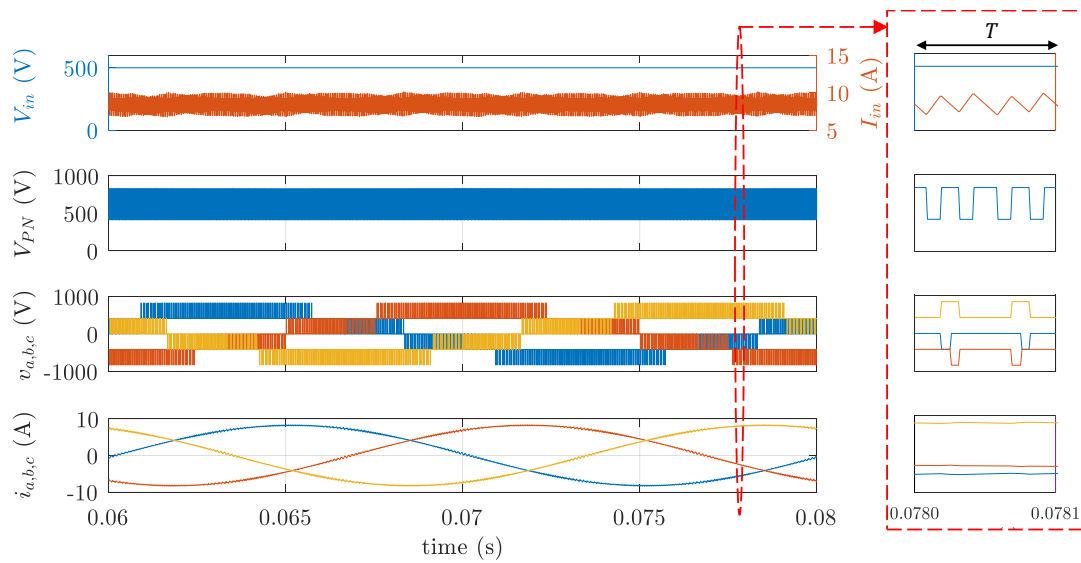


Figure 7. Simulation results for the UST/LST strategy, switching frequency 10 kHz, $m = 0.8$, and $D_0 = 0.2$. Left, top to bottom: input voltage (V_{in}) and input current (I_{in}); DC-link voltage (V_{PN}); and line-to-line voltages before filtering (v_{ab} , v_{bc} , and v_{ca}) and output currents (i_a , i_b , and i_c). Right: zoomed views for one switching cycle.

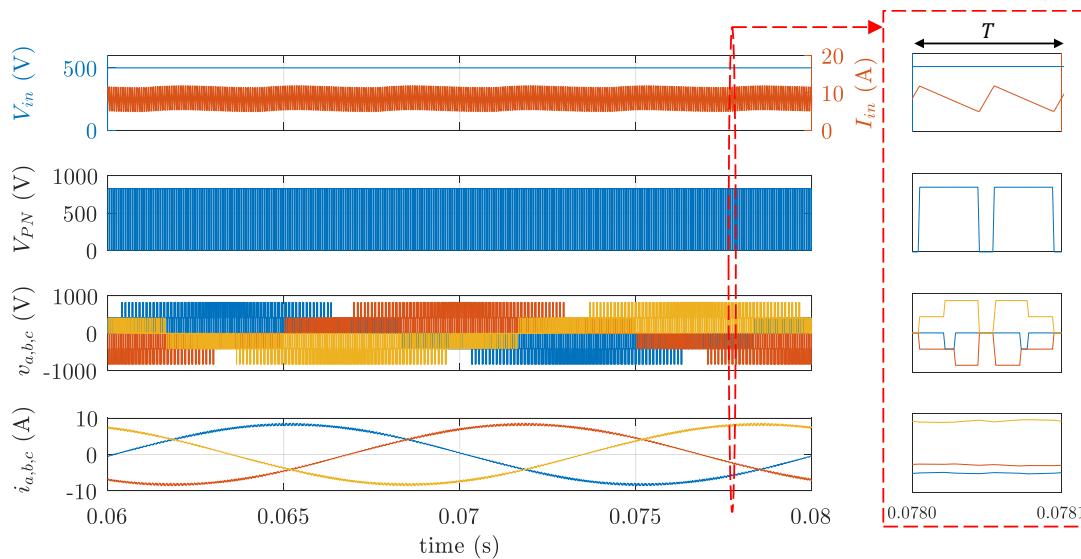


Figure 8. Simulation results for the FST strategy, switching frequency 10 kHz, $m = 0.8$, and $D_S = 0.2$. Top to bottom: input voltage (V_{in}) and input current (I_{in}); DC-link voltage (V_{PN}); and line-to-line voltages before filtering (v_{ab} , v_{bc} , and v_{ca}) and output currents (i_a , i_b , and i_c). Right: zoomed views for one switching cycle.

Observing Figures 7 and 8, some of the advantages obtained by using the new UST/LST strategy compared to the conventional FST strategy were directly proven. Switches S_1 and S_2 (see Figure 1) had to block V_{PN} . Thus, semiconductors with less blocking voltage capability were required, reducing the cost and the size of the power converter. For the same reason, less EMI can be expected. Hence, the complexity of the control and measurement systems was reduced substantially.

At the same time, switching losses were determined as the energy that a semiconductor needed to switch on and switch off. The lower the blocking voltage, the fewer the switching losses were expected. To illustrate switching loss improvement, simulation tests were conducted applying the two strategies for several values of ST duty cycle, D_0 for UST/LST and D_S for FST, where the modulation index was

set at $1 - D_0$ or $1 - D_S$, respectively. The influence of the switching frequency with constant D_S in the converter efficiency for UST and UST/LST was also studied. The load was the same as before (40 Ω in the wye connection), and the input voltage was adjusted according to D_0 or D_S to obtain the same output phase-to-neutral voltage (230 V) in all cases. The results, displayed in Figure 9, showed that the efficiency decreased with increasing ST duty cycle and with increasing switching frequency. However, the reduction was substantially lower for the proposed strategy. In other words, the new strategy exhibited lower global losses (conduction and switching). It is interesting to point out that this reduction mainly was due to switching loss decreases because the proposed strategy implied half the value of the semiconductor blocking voltage in the traditional strategy. Furthermore, for the same reason, semiconductor device stress was also reduced.

Voltage total harmonic distortion (THD), as a function of the D_0 or D_S , was measured. The quality of the output voltage was higher with the new UST/LST for any value of the shoot-through duty cycle. This fact was predicted by comparing the magnitudes of line-to-line voltages before filtering (v_{ab} , v_{bc} , and v_{ca}) from Figures 7 and 8.

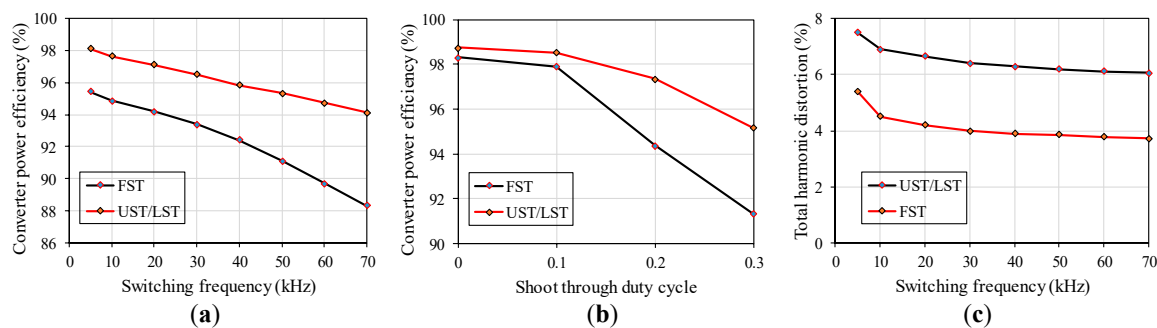


Figure 9. Performance comparisons between the classical FST strategy and the proposed UST/LST strategy: (a) Efficiency versus switching frequency; (b) Efficiency versus shoot-through duty cycle; (c) Total harmonic distortion versus switching frequency.

Table 3 sums up performance comparisons of UST/LST and FST strategies in terms of voltage THD (calculated up to 500 harmonics) before filtering, power efficiency, semiconductor stress, and the complexity of implementation, and it points out the advantages of the proposed strategy. In addition, the fact that this strategy was a carrier-based type also implied advantages in its practical implementation; therefore, it is a competitive alternative for quasi-Z-source T-type inverter modulation.

Table 3. Comparison of the new carried based UST/LST and the classical full shoot-through (FST) strategies.

| | Proposed UST/LST Strategy $m = 0.8; D_0 = 0.2$ | Conventional FST Strategy $m = 0.8; D_S = 0.2$ | Conventional UST/LST Strategy (Based on Space Vector Modulation) $m = 0.8; D_S = 0.2$ |
|---|---|---|--|
| Total Harmonic Distortion (%) up to 500 harmonics | 32.36 | 47.72 | 32.36 |
| Power Efficiency | High | Medium | High |
| Semiconductor Stress | Low | High | Low |
| Implementation Complexity | Low | Low | High |

4. Conclusions

The operating principles, circuit analysis, and modified new modulation carrier-based technique for a three-level T-type, quasi-Z-source inverter were presented. Using properly inserted short-circuits in the two halves of the DC-link voltage to the conventional three-level T-type inverter state sequence, the three-level T-type, quasi-Z-source inverter operated with voltage boosting capability and the correct volt-second average. This method was also simple to implement compared to the conventional

UST/LST SVM. The proposed idea was successfully validated by simulations for different inverter input voltages, which were taken as representative values of a photovoltaic system under variable weather conditions. Besides, the comparison was carried out with different shoot-through duty cycles and different switching frequencies. The improvement allowed reduction in waveform distortions and switching losses, which led to passive component rating reductions and increased reliability compared to previously reported methods.

Author Contributions: Conceptualization, F.B.-G., C.R.-C., and V.F.P.; Funding acquisition, F.B.-G., E.-G.R., and V.F.P.; Investigation, F.B.-G. and C.R.-C.; Methodology, M.I.M.-M. and O.H.; Software, C.R.-C. and O.H.; Supervision E.-G.R., MMM, and E.-R.C.; Validation, C.R.-C. and O.H.; Writing—original draft, F.B.-G.; Writing—review & editing, M.I.M.M., E.-G.R., and E.-R.C.

Funding: This work was supported by Junta de Extremadura (Regional Government), Spain, under the Mobility Scholarship Program for Teaching and Research Staff of the Autonomous Community of Extremadura 2018, by the fund for research group (GR18087) and the regional project (IB18067).

Acknowledgments: This work was also co-supported by the Spanish Agencia Estatal de Investigación (AEI) and Fondo Europeo de Desarrollo Regional (FEDER), under Project TEC2016-77632-C3-1-R (AEI/FEDER, UE), and through FCT under contracts UID/CEC/50021/2019, Pest-E/EEI/LA0021/2014 and UID/Multi/00308/2019.

Conflicts of Interest: The authors declare no conflict of interest.

References

- Schweizer, M.; Friedli, T.; Kolar, J.W. Comparative Evaluation of Advanced Three-Phase Three-Level Inverter/Converter Topologies against Two-Level Systems. *IEEE Trans. Ind. Electron.* **2013**, *60*, 5515–5527. [[CrossRef](#)]
- Xia, C.; Zhang, G.; Yan, Y.; Gu, X.; Shi, T.; He, X. Discontinuous Space Vector PWM Strategy of Neutral-Point-Clamped Three-Level Inverters for Output Current Ripple Reduction. *IEEE Trans. Power Electron.* **2017**, *32*, 5109–5121. [[CrossRef](#)]
- Choi, U.M.; Blaabjerg, F.; Lee, K.B. Control Strategy of Two Capacitor Voltages for Separate MPPTs in Photovoltaic Systems Using Neutral-Point-Clamped Inverters. *IEEE Trans. Ind. Appl.* **2015**, *51*, 3295–3303. [[CrossRef](#)]
- Schweizer, M.; Kolar, J.W. Design and implementation of a highly efficient three-level T-type converter for low-voltage applications. *IEEE Trans. Power Electron.* **2013**, *28*, 899–907. [[CrossRef](#)]
- Husev, O.; Stepenko, S.; Vinnikov, D.; Roncero-Clemente, C.; Romero-Cadaval, E. Single phase three-level neutral-point-clamped quasi-Z-source inverter. *IET Power Electron.* **2015**, *8*, 1–10. [[CrossRef](#)]
- Peng, F.Z. Z-source inverter. *IEEE Trans. Ind. Appl.* **2003**, *39*, 504–510. [[CrossRef](#)]
- Ellabban, O.; Abu-Rub, H. Z-Source Inverter: Topology Improvements Review. *IEEE Ind. Electron. Mag.* **2016**, *10*, 6–24. [[CrossRef](#)]
- Gao, F.; Loh, P.C.; Blaabjerg, F.; Vilathgamuwa, D.M. Performance evaluation of three-level Z-source inverters under semiconductor-failure conditions. *IEEE Trans. Ind. Appl.* **2009**, *45*, 971–981. [[CrossRef](#)]
- Anderson, J.; Peng, F.Z.Z. Four quasi-Z-Source inverters. In Proceedings of the 2008 IEEE Power Electronics Specialists Conference, Rhodes, Greece, 15–19 June 2008; pp. 2743–2749.
- Gupta, A.K.; Samuel, P.; Kumar, D. A state of art review and challenges with impedance networks topologies. In Proceedings of the 2016 IEEE 7th Power India International Conference, PIICON 2016, Bikaner, India, 25–27 November 2016; pp. 1–6.
- Husev, O.; Roncero-Clemente, C.; Romero-Cadaval, E.; Vinnikov, D.; Jalakas, T. Three-level three-phase quasi-Z-source neutral-point-clamped inverter with novel modulation technique for photovoltaic application. *Electr. Power Syst. Res.* **2016**, *130*, 10–21. [[CrossRef](#)]
- Husev, O.; Blaabjerg, F.; Roncero-Clemente, C.; Romero-Cadaval, E.; Vinnikov, D.; Siwakoti, Y.P.; Strzelecki, R. Comparison of Impedance-Source Networks for Two and Multilevel Buck–Boost Inverter Applications. *IEEE Trans. Power Electron.* **2016**, *31*, 7564–7579. [[CrossRef](#)]
- Roncero-Clemente, C.; Romero-Cadaval, E.; Pires, V.F.; Martins, J.F.; Vilhena, N.; Husev, O. Efficiency and loss distribution analysis of the 3L-Active NPC qZS inverter. In Proceedings of the 2018 IEEE 12th International Conference on Compatibility, Power Electronics and Power Engineering, CPE-POWERENG 2018, Doha, Qatar, 10–12 April 2018; pp. 1–6.

14. Ferñao Pires, V.; Cordeiro, A.; Foito, D.; Martins, J.F. Quasi-Z-Source Inverter with a T-Type Converter in Normal and Failure Mode. *IEEE Trans. Power Electron.* **2016**, *31*, 7462–7470. [[CrossRef](#)]
15. Panfilov, D.; Husev, O.; Khandakji, K.; Blaabjerg, F.; Zakis, J. Comparison of three-phase three-level voltage source inverter with intermediate dc–dc boost converter and quasi-Z-source inverter. *IET Power Electron.* **2016**, *9*, 1238–1248. [[CrossRef](#)]
16. Do, D.T.; Nguyen, M.K. Three-level quasi-switched boost T-type inverter: Analysis, PWM control, and verification. *IEEE Trans. Ind. Electron.* **2018**, *65*, 8320–8329. [[CrossRef](#)]
17. Abdelhakim, A.; Blaabjerg, F.; Mattavelli, P. Modulation Schemes of the Three-Phase Impedance Source Inverters-Part I: Classification and Review. *IEEE Trans. Ind. Electron.* **2018**, *65*, 6309–6320. [[CrossRef](#)]
18. Abdelhakim, A.; Blaabjerg, F.; Mattavelli, P. Modulation Schemes of the Three-Phase Impedance Source Inverters-Part II: Comparative Assessment. *IEEE Trans. Ind. Electron.* **2018**, *65*, 6321–6332. [[CrossRef](#)]
19. Effah, F.B.; Wheeler, P.; Clare, J.; Watson, A. Space-Vector-Modulated Three-Level Inverters with a Single Z-Source Network. *IEEE Trans. Power Electron.* **2013**, *28*, 2806–2815. [[CrossRef](#)]
20. Xing, X.; Zhang, C.; Chen, A.; He, J.; Wang, W.; Du, C. Space-vector-modulated method for boosting and neutral voltage balancing in Z-source three-level T-type inverter. *IEEE Trans. Ind. Appl.* **2015**, *2015*, 1621–1631. [[CrossRef](#)]
21. Shults, T.E.; Husev, O.; Blaabjerg, F.; Roncero-Clemente, C.; Romero-Cadaval, E.; Vinnikov, D. Novel Space Vector Pulsewidth Modulation Strategies for Single-Phase Three-Level NPC Impedance-Source Inverters. *IEEE Trans. Power Electron.* **2019**, *34*. [[CrossRef](#)]
22. Qin, C.; Zhang, C.; Chen, A.; Xing, X.; Zhang, G. A Space Vector Modulation Scheme of the Quasi-Z-Source Three-Level T-Type Inverter for Common-Mode Voltage Reduction. *IEEE Trans. Ind. Electron.* **2018**, *65*, 8340–8350. [[CrossRef](#)]
23. Qin, C.; Zhang, C.; Xing, X.; Li, X.; Chen, A.; Zhang, G. Simultaneous Common-Mode Voltage Reduction and Neutral-Point Voltage Balance Scheme for the Quasi-Z-Source Three-Level T-Type Inverter. *IEEE Trans. Ind. Electron.* **2019**. [[CrossRef](#)]
24. Roncero-Clemente, C.; Romero-Cadaval, E.; Ruiz-Cortes, M.; Husev, O. Carrier Level-Shifted Based Control Method for the PWM 3L-T-Type qZS Inverter with Capacitor Imbalance Compensation. *IEEE Trans. Ind. Electron.* **2018**, *65*, 8297–8306. [[CrossRef](#)]
25. Mohammadi, M.; Moghani, J.S.; Milimonfared, J. A Novel Dual Switching Frequency Modulation for Z-Source and Quasi-Z-Source Inverters. *IEEE Trans. Ind. Electron.* **2018**, *65*, 5167–5176. [[CrossRef](#)]
26. Noroozi, N.; Zolghadri, M.R. Three-Phase Quasi-Z-Source Inverter with Constant Common-Mode Voltage for Photovoltaic Application. *IEEE Trans. Ind. Electron.* **2018**, *65*, 4790–4798. [[CrossRef](#)]
27. Abdelhakim, A.; Davari, P.; Blaabjerg, F.; Mattavelli, P. Analysis and Design of the Quasi-Z-Source Inverter for Wide Range of Operation. In Proceedings of the 2018 IEEE 19th Workshop on Control and Modeling for Power Electronics, COMPEL 2018, Padua, Italy, 25–28 June 2018; pp. 1–6.
28. Pimentel, S.P.; Husev, O.; Vinnikov, D.; Roncero-Clemente, C.; Stepenko, S. An Indirect Model Predictive Current Control (CCS-MPC) for Grid-Connected Single-Phase Three-Level NPC Quasi-Z-Source PV Inverter. In Proceedings of the 2018 IEEE 59th International Scientific Conference on Power and Electrical Engineering of Riga Technical University (RTUCON), Riga, Latvia, 12–13 November 2018; pp. 1–6.
29. Loh, P.C.; Gao, F.; Blaabjerg, F.; Feng, S.Y.C.; Soon, K.N.J. Pulsewidth-Modulated Z-Source Neutral-Point-Clamped Inverter. *IEEE Trans. Ind. Appl.* **2007**, *43*, 1295–1308. [[CrossRef](#)]
30. Effah, F.B.; Wheeler, P.W.; Watson, A.J.; Clare, J.C. Quasi Z-source NPC inverter for PV application. In Proceedings of the 2017 IEEE PES PowerAfrica, Accra, Ghana, 27–30 June 2017; pp. 153–158. [[CrossRef](#)]
31. Liu, Y.; Abu-Rub, H.; Ge, B.; Blaabjerg, F.; Ellabban, O.; Loh, P.C. *Impedance Source Power Electronic Converters*; Wiley: Hoboken, NJ, USA, 2016; ISBN 9781119037118.
32. McGrath, B.P.; Holmes, D.G.; Lipo, T. Optimized Space Vector Switching Sequences for Multilevel Inverters. *IEEE Trans. Power Electron.* **2003**, *18*, 1293–1301. [[CrossRef](#)]

